RSC Sustainability

ROYAL SOCIETY OF CHEMISTRY

PAPER

View Article Online
View Journal | View Issue

Cite this: *RSC Sustainability*, 2024, **2**, 4036

Elucidating the role of the nanostructure in protein aerogels for removal of organic water pollutants†

Rodrigo Sanches Pires,[a] Antonio J. Capezza,[b] David Jonsson,[a] Jessica Lyrner Morén,[a] Mikael S. Hedenqvist[b] and Christofer Lendel *[a]

Access to efficient and affordable materials for water purification is of fundamental importance for the sustainable development of our society. Materials based on protein nanofibrils (PNFs) from agricultural waste- or side streams have recently been shown to have excellent adsorption properties for organic as well as inorganic pollutants. We here investigate the role of the nanostructure in aerogels made from whey protein isolate for the removal of a model pollutant (ibuprofen) from water. Water stable aerogels were produced using a recently developed approach for intrinsic crosslinking of protein materials without requiring additives. By comparing materials made from PNFs and from non-fibrillar whey protein we find that the fibrils have dual roles in enhancing the ibuprofen binding capacity. The PNFs do have a higher direct binding affinity but they also remodel the cell wall structures of the aerogels, resulting in a mesoporous network with enhanced ability of pollutant adsorption.

Received 3rd July 2024
Accepted 3rd November 2024

DOI: 10.1039/d4su00352g

rsc.li/rscsus

Sustainability spotlight

Efficient and inexpensive materials for remediation of polluted water could have significant impact on the environment and the quality of life. Nanostructured protein materials from abundant agricultural side streams have recently been highlighted as both sustainable and very efficient for water purification. We here investigate how the fibrillar protein nanostructures in these materials affect their performance. Our results show that the nanofibrils provide a higher binding affinity to the investigated pollutant but also remodel the microstructure of the material. Together these effects results in substantially higher adsorption capacity of the nanostructured material compared to materials from the same protein source without defined nanostructure.

Introduction

Water pollution is causing massive problems worldwide and the strive for clean water and sanitation for all is an important goal for a sustainable society. Water management is also strongly connected to many other sustainability aspects with substantial economic and social impacts.[1] The composition of polluted water can be very complex, with contributions from agricultural activities, industrial processes, and common households. Efficient remediation of multi-polluted water is challenging, and the required materials may be both expensive and produced by non-sustainable processes. Common water purification technologies include adsorption, distillation, ion exchange, chemical precipitation, coagulation–flocculation, oxidation, electrochemical treatment, membrane filtration, and biological treatment.[2,3] The adsorption approach is very attractive because of low investment costs and low energy consumption. The most employed adsorption material is activated carbon. Although this is considered an inexpensive material, the energy consumption for production and regeneration is extensive. Alternative adsorption materials from synthetic polymers or nanocellulose are associated with high costs for production and/or low sustainability of the materials' life cycles.[1]

Recently, protein nanomaterials, and in particular protein nanofibrils (PNFs), have emerged as a very promising solution for water purification with extremely high efficiencies for the removal of both organic[4–6] and inorganic[7–9] pollutants. The manufacturing of amyloid-like PNFs rely on the self-assembly of protein molecules (or peptide fragments from such molecules) and can be produced from a variety of abundant side streams from the agricultural sector, *e.g.* milk, soy or potato protein.[10,11] PNFs have been suggested to be less expensive and more sustainable than both activated carbon and cellulose nanofibrils for water purification applications.[1] Among the challenges in developing real water purification products from the PNF technology is the preparation of filter materials. Thin membranes (films) made directly from PNFs typically have a high degree of fibril packing and thereby low porosity.[12,13] The pioneering studies in the field involved composite materials of activated carbon and PNFs.[7] More recently, it was reported that PNF aerogels exhibited excellent efficiency for the removal of

[a]*Department of Chemistry, KTH Royal Institute of Technology, Teknikringen 30, SE-100 44, Stockholm, Sweden. E-mail: lendel@kth.se*

[b]*Department of Fibre and Polymer Technology, KTH Royal Institute of Technology, Teknikringen 56-58, SE-100 44, Stockholm, Sweden*

† Electronic supplementary information (ESI) available. See DOI: https://doi.org/10.1039/d4su00352g

organic pollutants from water[5] and for recovering gold from electronic waste.[9] However, the preparation of these aerogels relied on adding op to 37% w/w of crosslinking chemicals (butanetetracarboxylic acid and sodiumhypophosphate) to make the aerogels water resistant. We recently demonstrated a method to prepare water resistant PNF aerogels without any chemical additives by incubation at elevated temperatures (150 °C).[14] Interestingly, we found that the mechanical properties of these aerogels could be tuned by adjusting the time of the thermal treatment process. Hence, this approach could be very useful in the design of aerogel-based membranes for real water remediation applications.

So far, the results from several studies have clearly demonstrated the ability of whey protein PNFs to function as adsorbents in water purification applications[1] and that aerogels are a suitable format for such devices.[5,9] However, a critical comparison between whey protein in the form of nanofibrils and the same protein with other nanoscale characteristics has not been reported. Whey protein isolate (WPI) is easily transformed into PNFs by incubating the solution at pH 2 and 90 °C.[15,16] The fibrils are assembled by hydrolytic peptides originating from the protein β-lactoglobulin, which constitutes 50–60% of the protein content in the isolate.[17] The morphology of the formed PNFs can be controlled by the solution conditions[18] or by changing the initial concentration of WPI.[16] At low concentrations of WPI (below 40 g l^{-1}) the fibrils are straight (semi-flexible) and can reach lengths of several micrometers. At higher concentrations (above 60 g l^{-1}), they are instead short and curved (worm-like). The nanoscale morphology can substantially affect the structure and mechanical properties of the materials formed from the PNFs.[12,19]

We here use the common anti-inflammatory drug molecule ibuprofen as a model organic pollutant. Ibuprofen is one of the most used over-the-counter drugs worldwide[20] and therefore, released in large amounts to aquatic ecosystems *via* community wastewater. It has been reported that ibuprofen is harmful to marine life even at concentrations as low as 10–100 ng l^{-1},[21,22] values that are within the range of measured concentrations for ibuprofen found in surface waters.[23,24] Ibuprofen can reduce the movement activity of freshwater organisms, such as *Gammarus pulex*,[25] and have detrimental fitness effects in *Rhamdia quelen*.[26] Previous studies have shown that ibuprofen can be removed from water by β-lactoglobulin aerogels.[5]

In the work presented here, we compare the binding of ibuprofen to fibrillar and non-fibrillar whey protein; first in solution/dispersion and then as the adsorption‡ capacity of aerogels derived from four different manufacturing protocols. The results provide knowledge about the roles of the protein nanostructure as well as the aerogel microstructure as a future sustainable material for removing pollutants from wastewater. Our findings corroborate the positive impact of the PNFs on the adsorption capacity and indicate that the effect originates from a combination of the structural features of the PNFs and a higher porosity of the cell walls in the gel network.

‡ We will use the term adsorption throughout this text although the nature of the sorption processes in the aerogels has not been fully assessed.

Results and discussion

Binding of ibuprofen to fibrillar and non-fibrillar whey protein

As a first experiment, we compared the binding of ibuprofen to whey protein in solution, either in the form of PNFs or in non-fibrillar form. Two morphologies of PNFs, curved and straight,[16,19] were included in the study to elucidate if fibril morphology affects the binding, and the experiments were conducted using micro-dialysis with a 5 kDa cut-off membrane. Ibuprofen was added to a solution of purified PNFs (0.15 g l^{-1}) or dissolved WPI (0.15 g l^{-1}) and placed in one of the chambers in the dialysis device. The other chamber was filled with deionized water. The ibuprofen concentration in the second chamber was then measured after incubation for 24 h at 25 °C on a nutating mixer. The results (Fig. 1A) show that the ibuprofen concentration in the second chamber is significantly lower when protein is present in the first chamber, compared to the control experiment without any protein. The free ibuprofen concentration with non-fibrillar WPI added is about 40% of the control, while the corresponding values are 24% and 8% for curved and straight PNFs, respectively. The amount of bound

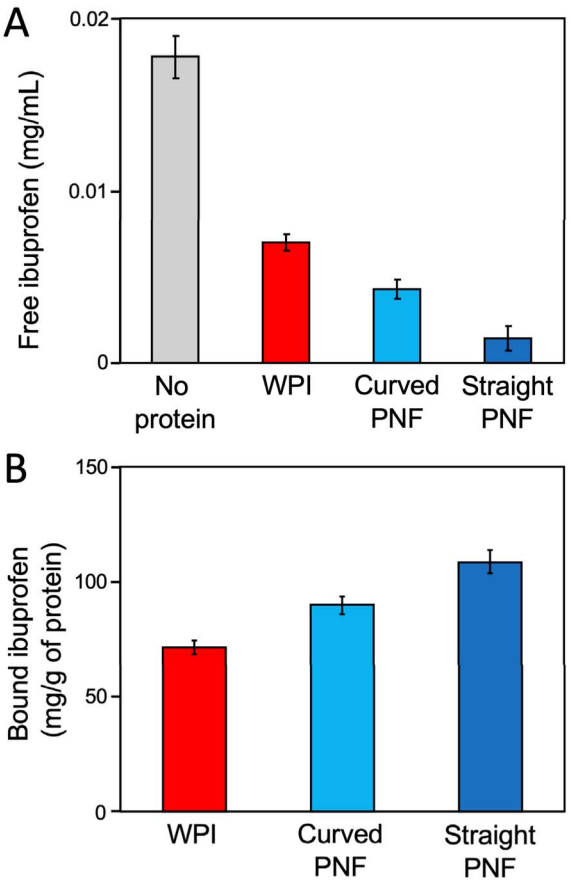

Fig. 1 Binding of ibuprofen to fibrillar and non-fibrillar whey protein investigated by equilibrium microdialysis. (A) The diagram shows how much ibuprofen was found in chamber 2 after the experiment. (B) Estimated specific binding capacities of the proteins derived from the equilibrium microdialysis experiment.

ibuprofen per gram protein can be estimated using the assumption that the concentration of free ibuprofen is the same in both dialysis chambers. The results show that the protein binds between 70 and 110 mg ibuprofen per gram of protein and that the nanofibrillar forms bind more than the non-fibrillar WPI (Fig. 1B). These values are in the same order of magnitude as previously reported adsorption capacities of PNF aerogels.[5] Hence, we conclude that whey proteins have a substantial binding capacity for ibuprofen and that the ordered nanostructure of the PNFs enhances the binding. The advantage of ordered structures is further illustrated by the straight fibrils binding more ibuprofen than the curved PNFs.

Preparation of protein aerogels

The manufacturing process of the PNF aerogels explored in this study is summarized in Fig. 2. Fibril formation is achieved by dissolving the WPI powder at pH 2 and heating the solution to 90 °C. In previous work, we observed that adding pre-formed PNFs (seeds) to the WPI solution before fibrillation results in a transition of the solution into a hydrogel, even at relatively low protein concentrations.[16,27] Notably, without the added seeds, gels are not formed within the typical experimental time (3–4 days). With optimized solution conditions, the sol–gel transition can take place within an hour, significantly reducing the need for extended incubation times at high temperatures and the energy used in the process. We here use the hydrogels as a starting point to produce aerogels and compare materials formed using PNF seeds of the two different morphologies, straight (PNF-S) and curved (PNF-C), respectively. The fibrillar structures of the formed gels are illustrated in ESI Fig. S1.†

Aerogels were produced by lyophilization after freezing the hydrogels at −80 °C. The freeze-dried structures are very brittle and thereby difficult to handle in any application. They are also very water sensitive and easily disintegrate upon rehydration. In previous studies, aerogels for water purification were cross-linked by butanetetracarboxylic acid and sodiumhypophosphate.[5] We here use the recent discovery that intrinsic isopeptide crosslinks can form between whey PNFs upon heating the aerogels at 150 °C. This treatment significantly improves the mechanical properties and stability in wet environments (ESI Fig. S2†).

To explore the role of the amyloid-like nanostructure, we compared PNF-based aerogels with two classes of non-PNF aerogels produced from the same WPI raw material. The first type of material (NF-5) is formed by heating the WPI solution close to the isoelectric point (pH 5.1)[12,19]. This treatment results in non-transparent particulate hydrogels,[17] which may display some amyloid-like molecular features[28] but do not have the fibrillar characteristics of the PNFs formed at lower pH. The second type of non-PNF material (NF-7) was produced by reducing the disulfide bonds in native whey proteins at neutral pH followed by heating the solution. This results in a transparent hydrogel upon cooling, presumably formed by denatured protein chains. Both classes of non-PNF hydrogels were freeze-dried in the same way as the PNF-based materials. The particulate NF-5 material was also heat-treated to create cross-links. The NF-7 material was not further heat treated as it appeared to form new (disulfide) cross-links during the gelation process. It was indeed found to be as water stable as the other three materials. The appearance of the final aerogels of the four classes of materials studied here, *i.e.* PNF aerogels seeded by either straight or curved PNFs, non-fibrillar particulate gels formed at the isoelectric point and non-fibrillar aerogels formed under reducing conditions at neutral pH, are shown in the ESI Fig. S2.†

Removal of ibuprofen from water

The four classes of materials were investigated for the removal of ibuprofen from water solution. To avoid interference from protein fragments leaking from the aerogels, all materials were thoroughly washed by submerging them in pure water before they were exposed to ibuprofen solution. Hence, the materials used in the removal experiments were rehydrated aerogels and the measured adsorptions correspond to the equilibration process between pure water inside the gel structures and ibuprofen-containing water in the surrounding.

The adsorption of ibuprofen by the aerogels was measured in triplicates. Each aerogel sample was placed in 50 ml ibuprofen solution with a 30 mg l^{-1} concentration. The concentration was selected to allow spectroscopic quantification of ibuprofen and although it is higher than typical levels in polluted water it is suitable for comparison of the adsorption in the different materials. Additionally, for all types of aerogels, one control experiment in which the aerogels were placed in 50 ml pure water was performed to measure any background from released protein. The solutions were analyzed spectroscopically, and the remaining ibuprofen in the solution were determined from the absorbance at 222 nm. The remaining concentration of

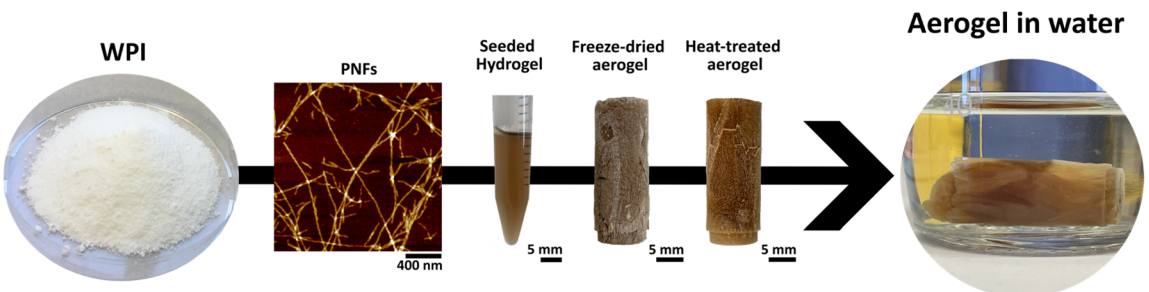

Fig. 2 Overview of the process for manufacturing heat-treated (intrinsically cross-linked) aerogels.

ibuprofen was analyzed after 24 h and after 72 h. The aerogels were then dried to determine their mass.

Fig. 3 illustrates that there is a time-dependent uptake of ibuprofen in the materials. This is likely due to the molecular diffusion of ibuprofen into the pores followed by adsorption to the cell walls. Adsorption appear to be the most obvious mechanism which is supported by the binding studies in solution described above as well as the well-known ability of various organic compounds to bind to the surface of PNFs.[10] However, we cannot exclude molecular absorption into the porous cell wall structures (*vide infra*), which agrees with the ibuprofen molecule being slightly polar while the protein matrix is plasticized by the water. The amounts of adsorbed ibuprofen at the two time points are shown in Fig. 3. After 24 h, it can be observed that the aerogels made up of PNFs have adsorbed more ibuprofen than the non-PNF aerogels, with the PNF-S aerogel adsorbing the most. Among the non-PNF materials, the NF-7 aerogel adsorbed more ibuprofen than the NF-5 aerogel. Interestingly, after 24 h the PNF gels continue to adsorb more ibuprofen while the non-PNF aerogels appear saturated. The results after 72 h show a clear difference in adsorption capacity between the PNF-based aerogels and the non-PNF materials. We also observe distinct performances of the PNF aerogels seeded from straight and curved fibrils, respectively. Hence, the nanostructure of the WPI aerogels do have a substantial role for their performance in water purification applications. However, it is unclear if the magnitude of different adsorption properties results from the different protein nanostructures, the aerogel microstructure, or the cumulative phenomena of both variables. It is expected that diffusion properties for the different aerogels will be highly dependent on the aerogel network and porous structure. Although the adsorption capacities of the aerogels agree with the relative order of the binding capacities in solution (Fig. 1) the amount of bound ibuprofen is much lower per gram of material in the aerogel state. The measured values are also lower than the adsorption capacities reported by Peydayesh *et al.*[5] Hence, the available protein surface for ibuprofen binding is significantly decreased in the aerogels compared to the protein in the solution.

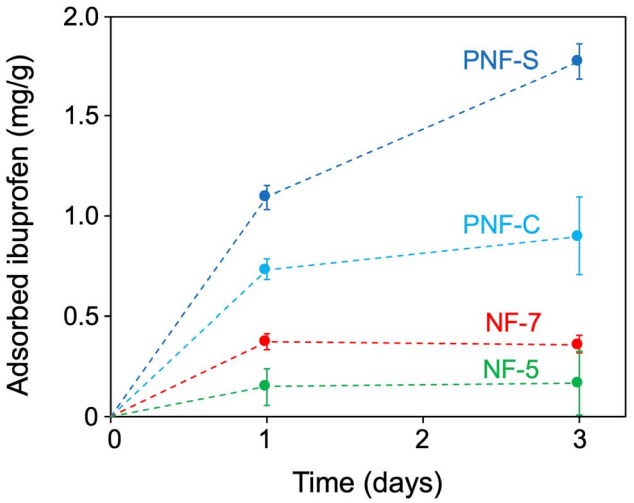

Fig. 3 Adsorbed amounts of ibuprofen (mg ibuprofen per gram gel) after 1 day and 3 days storage in ibuprofen solution. Data points are shown with ± one standard deviation from three replicates.

Comparison of accessible pore volume

The diffusion process of ibuprofen into the wet aerogel is controlled by pore size, the distribution of open and closed pores and the degree of connection between pores. A modified Archimedes principle method with *n*-hexane was used to measure porosity and the fraction of open pores. The solvent, *n*-hexane, itself is hydrophobic and does not swell the protein cell walls.[29] The capillary uptake of *n*-hexane was dominating the process, yielding an essentially momentaneous uptake when immersed in *n*-hexane. This shows that the networks of the materials has good interconnectivity and allowed us to rapidly measure the mass of the aerogels immersed in liquid (m_i) and thereby calculate the porosity related to closed pores (Table 1). The open and closed porosity of the NF-7 sample could not be determined since the samples were floating in *n*-hexane. This fact and that the uptake (w) was smaller than for the NF-5 sample with similar density indicated a sizeable amount of closed pores in NF-7. The density of NF-7 was calculated based on the mass and volume (using a caliper) of the samples. The results (Table 1) show that the porosity of the materials is above 90% and comparable to, for example, previously investigated chitosan/wheat gluten blends.[30] There is also some differences between the investigated aerogel materials with the two PNF-based aerogels having higher uptake than the non-fibrillar variants. Comparing the two PNF-based aerogels, the material made from curved seeds has a higher porosity than straight seeds. We don't find a strong correlation between the ibuprofen binding and the uptake/porosity parameters (all $R^2 < 0.4$) indicating that the accessible pore volume is not the main determinant for the adsorption capacity. This conclusion refers to the microscale pore volume, as *n*-hexane is not expected to penetrate the cell walls.

Comparison of the aerogel microstructures

The microstructure of the aerogels was further investigated by SEM (Fig. 4) and we observe substantial morphological differences between the materials. The NF-5 aerogel (Fig. 4C)

Table 1 Data from porosity measurements using Archimedes method. ρ_f: density, P_o: open porosity, P_c: closed porosity, P_t: total porosity, w: uptake of *n*-hexane. The values are the averages and standard deviations of triplicates

Material	ρ_f (kg m^{-3})	P_o (%)	P_c (%)	P_t (%)	w (%)
PNF-S	94 ± 23	91.3 ± 3.1	1.6 ± 1.2	93.0 ± 1.7	666 ± 172
PNF-C	65 ± 5	94.3 ± 0.4	0.9 ± 0.7	95.2 ± 0.4	965 ± 77
NF-5	109 ± 26	87.4 ± 3.0	4.5 ± 1.2	91.9 ± 1.9	554 ± 152
NF-7	109 ± 10	ND[a]	ND[a]	91.8 ± 0.8	499 ± 140

[a] Values could not be determined since the sample was floating in *n*-hexane.

comprises an interpenetrated network of agglomerates, which agrees with the particulate gels that are expected to form close to the isoelectric point.[17] No continuous cell walls are observed, which makes the microstructure fundamentally different than the other three materials. The other non-PNF gel, NF-7, forms very flat and smooth cell walls (Fig. 4D). The direction of the ice crystals from the lyophilization process can be followed easily. This directionality is an interesting property that can be crucial in applications such as thermal insulators for instance[31] but here it appears to be associated with a lower degree of open porosity than the other materials (Table 1). The cell structure of the PNF-S aerogel (Fig. 4A) has similarities with the NF-7 material (Fig. 4D) but it is more difficult to define the cells. The cell walls wrinkle into nerve-like structures, which may originate from the PNFs. Despite the rather similar preparation protocol, the PNF-C aerogel appears different (Fig. 4B). Here, fewer "nerves" are observed, and the cellular structure is much more evident.

A closer look at the cell walls reveals some interesting differences (Fig. 4, right column; ESI Fig. S3.†). Since the NF-5 material had a completely different architecture, the image in Fig. 4C is primarily shown as a reference with a similar resolution. In general, the PNF-based materials (Fig. 4A and B) have thicker and rougher cell walls than the NF-7 sample (Fig. 4D). Moreover, the cross sections of the cell walls in the PNF-materials display a porous network with pore sizes below 100 nm. This apparent pore size seems to be lower than the ones observed in the native hydrogel structure,[27] which elucidates the role of the lyophilization process in compressing the PNFs in their original entangled conformation into higher hierarchally-aggregated structures. The NF-7 sample, on the other hand, seems to have more compact walls without any density variations. Hence, the highly porous network at the nanoscale could trigger encapsulation/adsorption of low molecular weight substances.

Structural characterization by small angle X-ray scattering

To investigate the structural properties of the cell walls in more detail, we performed SAXS experiments on thin (1–2 mm) specimens cut out from the dry aerogels. The 2D scattering profiles all display some degree of anisotropy (Fig. 5), which agrees with the anisotropic pore structures seen by SEM. The

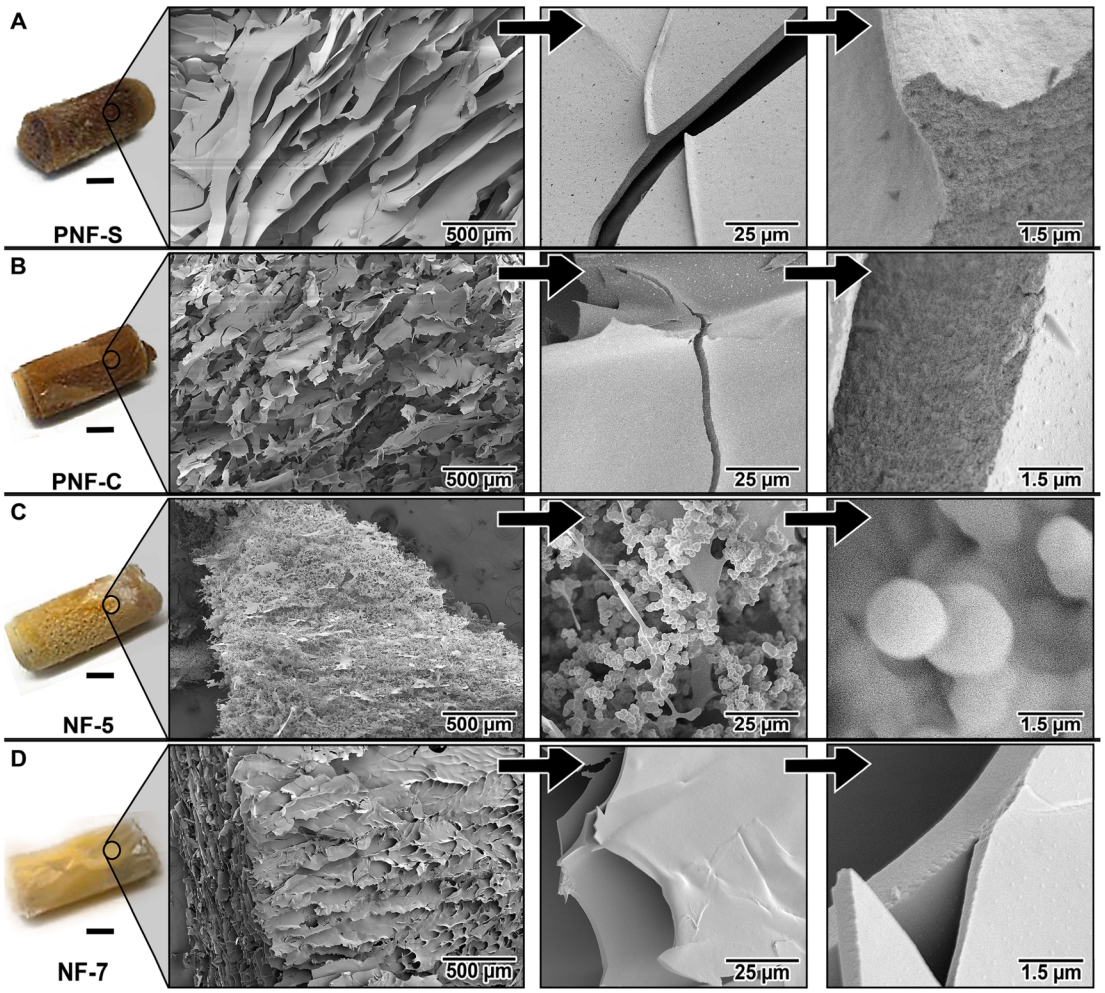

Fig. 4 SEM images of the four classes of aerogels. (A) PNF-S aerogel from straight seeds. (B) PNF-C aerogel from curved seeds. (C) NF-5 aerogel formed at the isoelectric point. (D) NF-7 aerogel formed at neutral pH under reducing conditions. The scale bar in the left column is 5 mm.

origin of this directional order is most likely due to the water crystallization during sample freezing, as the native hydrogel structure is formed by physical entanglements of the fibrils with globally isotropic arrangements.[27] Fitting the data in the low q region to a Porod-type power law reveals typical q^{-4} relationships for the two nonfibrillar materials. However, both the PNF aerogels have exponents higher than −4: −3.3 and −3.6 for PNF-S and PNF-C, respectively. This indicate cell wall structures with higher roughness (higher fractal dimension),[32] which agree with the more complex wall structure seen in the SEM images.

The integrated scattering curves are shown in Fig. 5. There are distinctive features of the two PNF-based materials as there are increased scattering intensities in the q-range of 0.2 to 1.0 nm^{-1}. These features become even more evident in the Kratky plot (Fig. 6). The PNF-based aerogels display peaks in the region expected for a mesoporous network with pore sizes below

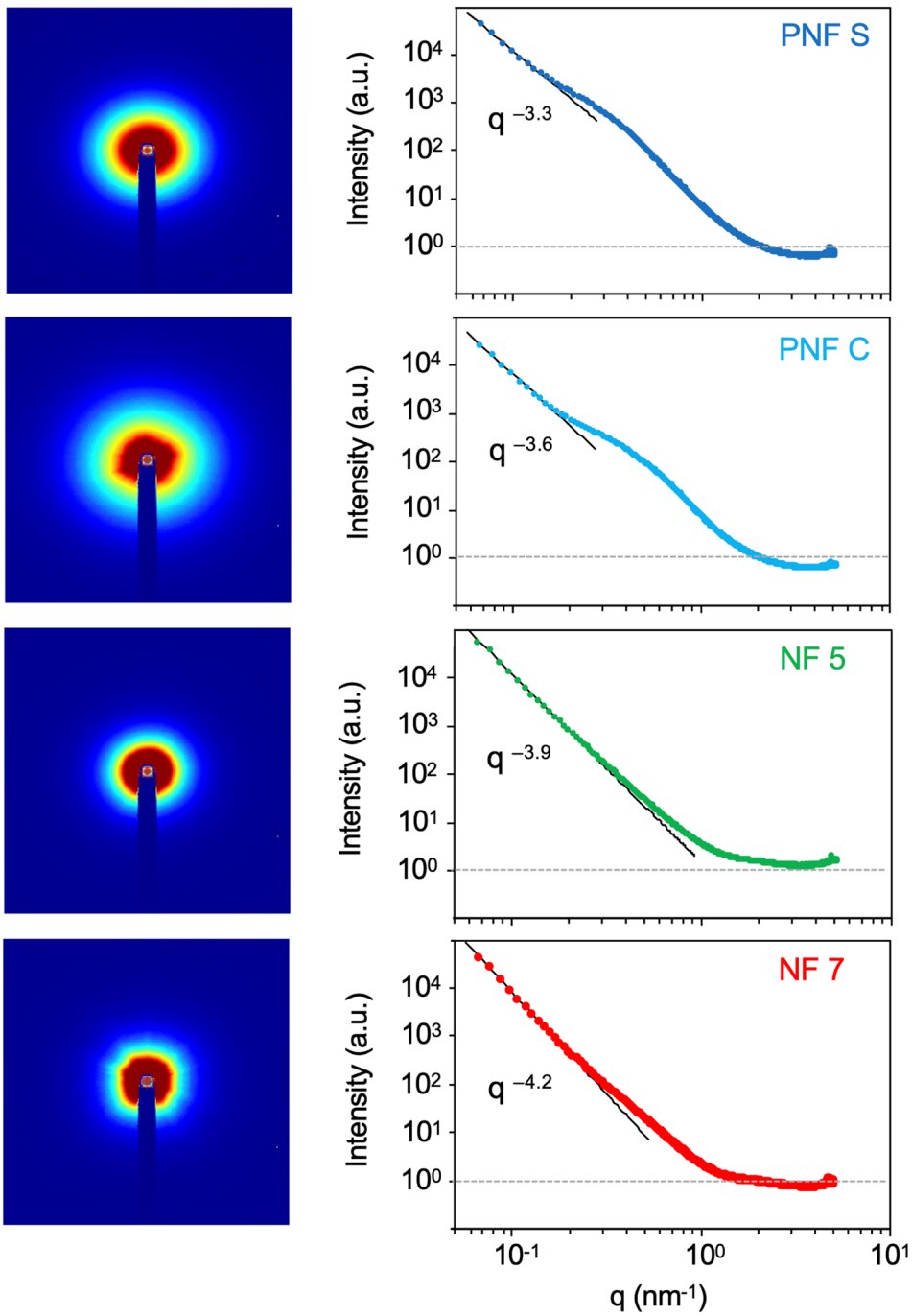

Fig. 5 2D SAXS patterns (left) and the corresponding linear scattering profiles (right) of the four investigated aerogels. The fitted Porod power laws at low q-values are indicated.

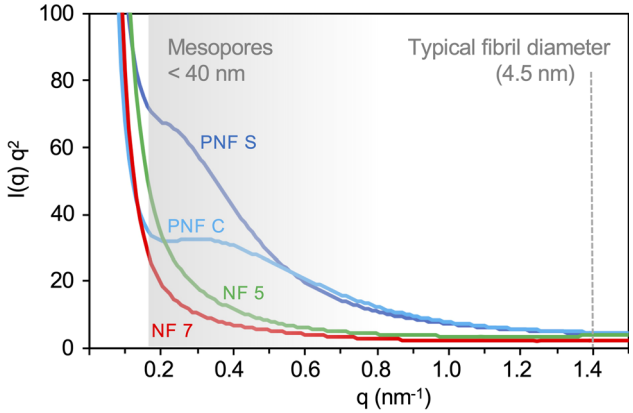

Fig. 6 Kratky plot of the SAXS data for of the four investigated materials. The size range of mesopores is indicated by the gray shading and the q-value corresponding to typical PNF diameters are marked for comparison.

40 nm. Similar peaks are not found in the non-fibrillar materials. It should be noted that the full thickness of the cell walls is much larger than this distance (see Fig. 4), and the thickness of individual fibrils (around 4.5 nm)[27] is expected at higher q-values (>1.0 nm^{-1}). The scattering profiles for the NF-7 and NF-5 aerogels are similar and without any prominent features in the Kratky plot (Fig. 6). The main difference is that the NF-5 curve shows a slightly slower decay.

Conclusions

In this work, we have investigated the role of the nanostructure for protein-based aerogels intended for water purification applications. We find that the ordered structure found in amyloid-like PNFs derived from whey enhances the intrinsic binding of the model pollutant, ibuprofen. This effect could be related to a higher fraction of hydrophobic surface area displayed by the PNFs compared to the non-fibrillar protein states. The repetitive charge distribution of the PNFs may also favor specific electrostatic interactions with organic molecules.[33] Interestingly, the difference in adsorption capacity is not the only favorable effect of the nanofibrils. The PNF-based aerogels have cell walls with apparent mesoporous structures, which may be accessible to small pollutant molecules. Such a mechanism agrees with the continued uptake of ibuprofen by the PNF materials after the first 24 h, which is not observed for the non-fibrillar aerogels. The porous wall structure may be a result of a stronger (stiffer) hydrogel network formed by the PNFs compared to the network formed by non-fibrillar species. When ice crystals are formed and the gel network is reshaped during the freezing process, the cell wall keeps some porosity, while the weaker network formed by single protein chains (NF-7) collapses in the walls. Aerogels formed from particulate gel networks (NF-5) have a fundamentally different microstructure and most likely expose fewer binding sites for ibuprofen as they may be hidden inside the particulates. Given the large difference between ibuprofen binding to proteins in solution and the adsorption capacity of the aerogels, there should be room for major improvements in the aerogel manufacturing process to achieve a higher accessible surface area for the pollutants.

Experimental section

Materials

Whey protein isolate (WPI, Lacprodan Di-9224) was kindly provided by Arla Food Ingredients. Ibuprofen sodium salt (analytical grade, <98% pure) was purchased from Merck Life Science AB. Concentrated hydrochloric acid and sodium chloride was from Sigma-Aldrich, *n*-hexane from VWR BDH chemicals, and ditiotreitol (DTT) was from BioChimica (all analytical grade).

Fibril preparation

To prepare PNFs, WPI was dissolved to a concentration of approximately 120 mg ml^{-1} in 0.1 M HCl. The pH of the solutions was adjusted to 2 by adding 2 M HCl. The solution was then dialyzed against 10 mM HCl (pH 2) using a dialysis membrane with 6–8 kDa cut-off (Spectrum laboratories). The concentration of WPI was adjusted to 40 mg ml^{-1} to obtain straight fibrils or to 60 mg ml^{-1} to obtain curved fibrils. PNFs were formed during incubation of the samples at 90 °C under quiescent conditions for 48 h and then purified using dialysis against 10 mM HCl (pH 2) with a 100 kDa cut-off dialysis membrane (Spectrum laboratories).

Aerogel preparation

Four types of aerogels were made for this study. Two were derived from seeded PNF hydrogels created at pH 2 (PNF-S and PNF-C). The other two types were non-PNF aerogels, one produced close to the isoelectric point (NF-5) and the other made at pH 7 under reducing conditions (NF-7). Seeds (*i.e.* fragmented fibrils) were produced from the purified PNFs by sonication using a tip ultrasonicator (Qsonica Q500) equipped with a 6 mm micro tip. The amplitude was 20% and sonication was done in pulses (2 s on, 10 s off) for a total effective time of 1 min. During the process, the sample was immersed in a water bath. PNF hydrogels were produced from dialysed WPI solution (40 mg ml^{-1}) with 10% straight or curved seeds mixed in plastic tubes at pH 2 (HCl) and 0.1 M NaCl. The solutions were then incubated at 90 °C for 24 hours to ensure hydrogel formation. The tubes with the hydrogels were placed in a freezer at −80 °C for 24 hours and then lyophilized in a vacuum chamber for 24 h. Finally, the dry aerogels were heat-treated in at 150 °C for 7 days. The non-PNF aerogel prepared close to the isoelectric point (NF-5) was produced from WPI dissolved in water to a concentration of 50 mg ml^{-1}. The pH was adjusted to 5.1 using acetic acid and the solution was heated to 90 °C for 60 min. When cooled down to room temperature, opaque hydrogels were formed. The hydrogels were frozen at −80 °C for 24 hours, lyophilized under vacuum for 24 h and then heat-treated at 150 °C for 7 days. The non-PNF aerogel prepared under reducing conditions at pH 7 (NF-7) was produced from WPI dissolved in water to a concentration of 50 mg ml^{-1} with the addition of 30 mg ml^{-1} DTT. The solutions were incubated

for 60 min at 90 °C and then cooled to room temperature to form hydrogels. The hydrogels were frozen at −80 °C for 24 hours and lyophilized in a vacuum chamber for 24 h. These aerogels were stable in water without further treatment.

Microdialysis experiments

To determine the amount of ibuprofen bound to protein in solution, we used fast micro-equilibrium dialysis with equipment from Harvard Apparatus, USA. Here, two chambers of 500 μl each (designated chamber 1 and chamber 2) are separated by a 5 kDa dialysis membrane (Harvard Apparatus, USA). Three different samples were studied: curved fibrils, straight fibrils and non-fibrillar WPI. Both straight and curved PNFs were prepared at pH 2 and 90 °C as described above. After fibrillation, the samples were dialyzed against 10 mM HCl and stored in a refrigerated environment until further use. For the non-fibrillar WPI sample, WPI was dissolved in 10 mM HCl and dialyzed against the same solvent. All samples were diluted in 10 mM HCl to a stock concentration of 15 g l^{-1}. The protein solutions were further diluted to 0.15 g l^{-1} in distilled water for the microdialysis experiments. This was the initial protein concentration in chamber 1, where ibuprofen was also added. The low protein and ibuprofen concentrations ensure fast equilibrium while getting a good absorbance signal. As the membrane is impermeable to the fibrils and WPI, only ibuprofen flows into chamber 2, which is initially filled with distilled water. Dialysis is then performed for 24 h at 25 °C in a nutating mixer. The time was selected to ensure equilibrium. We performed the same experimental setup without ibuprofen to ensure no interference from any fibril/protein degradation at neutral pH. We measured the absorbance at 222 nm in chamber 2 and subtracted these values as backgrounds when ibuprofen is present. To ensure that the incubation time is sufficient for the equilibration of ibuprofen in both chambers, we performed the same experimental setup with ibuprofen in chamber 1 in the absence of protein. A total of 3 replicates per sample were performed. At equilibrium, the concentration of bound ibuprofen $[I_b]$ was calculated as:

$$[I_b] = [I_i] - 2[I_{\#2}] \quad (1)$$

where $[I_i]$ refer to the initial ibuprofen concentration in chamber 1 (20 mg l^{-1}) and $[I_{\#2}]$ refer to the final concentration of free ibuprofen in chamber 2.

Ibuprofen removal experiments

All aerogels were thoroughly washed in deionized water before the experiments to remove protein residuals that could be released and interfere with the UV absorption measurements. Tests on selected materials after the purification showed that the background absorption at 222 nm was less than 0.05 a.u. Still, to compensate for this, one gel of each type was incubated in pure water for the same time as those in the ibuprofen adsorption experiments. The UV absorptions of these solutions were subtracted from the measured absorption of ibuprofen. For the water purification experiments, each aerogel was placed in a 50 ml solution of 30 mg l^{-1} ibuprofen in Milli-Q water. Each type of material was investigated in triplicates. The solutions were analyzed after 24 h and 96 h. All the aerogels were then dried and weighted to determine their mass. The concentration of free ibuprofen was measured from UV absorption at 222 nm using a Cary300 Bio UV-vis spectrophotometer (Varian). The extinction coefficient of ε_{222} = 0.0345 cm^{-1} mg^{-1} l was determined from a calibration curve of ibuprofen in water.

Porosity measurements

The porosity of the aerogels (using triplicate specimens) were determined with a modified Archimedes principle method where the mass of the aerogels was determined in air (m_a), when immersed in liquid (*n*-hexane, m_i) and in the wet state (m_w) directly when removed from the liquid.[34] The values were corrected for *n*-hexane on the surface of the samples, leading to a factor of 3.2% lower final m_w-values. Based on these masses different volumes were determined. The volume of the polymer matrix was determined as:

$$V_m = \frac{m_a}{\rho_m} \quad (2)$$

where ρ_m is the density of WPI (1340 kg m^{-3}, ref. 14) The volume of open pores is calculated as:

$$V_o = \frac{m_w - m_a}{\rho_l} \quad (3)$$

where ρ_l is the density of *n*-hexane (660 kg m^{-3}, https://merckmillipore.com). The volume of closed pores is determined from:

$$V_c = \frac{m_a - m_i}{\rho_l} - V_m \quad (4)$$

The density of the aerogel is finally obtained as:

$$\rho_f = \frac{m_a}{V_t} \quad (5)$$

where $V_t = V_m + V_o + V_c$. The open porosity is calculated as:

$$P_o = \frac{V_o}{V_t} \times 100 \quad (6)$$

The closed porosity is:

$$P_c = \frac{V_c}{V_t} \times 100 \quad (7)$$

And, consequently, the total porosity is $P = P_o + P_c$. The liquid uptake is determined as:

$$w = \frac{m_w - m_a}{m_a} \times 100 \quad (8)$$

SEM imaging

The microstructure of the dry aerogels was imaged using a field-emission scanning electron microscope (FE-SEM, Hitachi

S4800, Japan). The freeze-dried materials were immersed in liquid nitrogen for 5 min and cryo-fractured inside the liquid nitrogen to ensure a cryogenic fracture. The fragments of the aerogels were placed carefully on carbon tape and sputtered using a gold target for 3 min, leaving a coating layer of *ca.* 2–3 nm. The microstructure images were taken using an acceleration voltage of 3 kV.

SAXS experiments

SAXS (small angle X-ray scattering) measurements were performed on an Anton Paar SAXSpoint 2.0 system (Anton Paar, Graz, Austria) equipped with a microsource X-ray (Cu Kα radiation, wavelength 0.15418 nm) and a Dectris 2D CMOS Eiger R 1 M detector with 75 εm by 75 μm pixel size. All measurements were performed with a diameter beam size of about 500 μm, at a sample stage temperature of 25 °C with a beam path pressure of 1–2 mbar. The sample to detector distance (SDD) was 564.5 mm. Samples were mounted on a multi-solid-sample holder mounted on a heated sampler and a VarioStage (Anton Paar, Graz, Austria), and samples were exposed to vacuum during measurement. 6 frames of 30 min duration were recorded, giving a total measurement time of 3 h per sample. The transmittance was determined and used for scaling the scattering intensities. Binning used to generate graphs was 500 data points. The software used for instrument control was SAXSdrive version 2.01.224 (Anton Paar, Graz, Austria), and post-acquisition data processing was performed using the software SAXSanalysis version 3.00.042 (Anton Paar, Graz, Austria).

Data availability

Data for this article will be made available at Zenodo.

Conflicts of interest

There are no conflicts to declare.

Acknowledgements

We thank the Åforsk foundation (Grant Number 22-36 to C. L. and M. H.), Formas (Grant Number 2022-00362 to A. J. C.) and the Treesearch Research Infrastructure access program for financial support. Helena Lennholm is acknowledged for student supervision and Jasna Stevanic Srndovic for performing the SAXS experiments.

References

1 M. Peydayesh and R. Mezzenga, *Nat. Commun.*, 2021, **12**, 3248.
2 A. Ahmad, S. H. Mohd-Setapar, C. S. Chuong, A. Khatoon, W. A. Wani, R. Kumar and M. Rafatullah, *RSC Adv.*, 2015, **5**, 30801–30818.
3 S. Bolisetty, M. Peydayesh and R. Mezzenga, *Chem. Soc. Rev.*, 2019, **48**, 463–487.
4 D. Morshedi, Z. Mohammadi, M. M. Akbar Boojar and F. Aliakbari, *Colloids Surf., B*, 2013, **112**, 245–254.
5 M. Peydayesh, M. K. Suter, S. Bolisetty, S. Boulos, S. Handschin, L. Nyström and R. Mezzenga, *Adv. Mater.*, 2020, **32**, 1907932.
6 T. Jin, M. Peydayesh, H. Joerss, J. Zhou, S. Bolisetty and R. Mezzenga, *Environ. Sci.: Water Res. Technol.*, 2021, **7**, 1873–1884.
7 S. Bolisetty and R. Mezzenga, *Nat. Nanotechnol.*, 2016, **11**, 365–371.
8 S. Bolisetty, N. Reinhold, C. Zeder, M. N. Orozco and R. Mezzenga, *Chem. Commun.*, 2017, **53**, 5714–5717.
9 M. Peydayesh, E. Boschi, F. Donat and R. Mezzenga, *Adv. Mater.*, 2024, **36**, 2310642.
10 C. Lendel and N. Solin, *RSC Adv.*, 2021, **11**, 39188–39215.
11 M. Peydayesh, M. Bagnani, W. L. Soon and R. Mezzenga, *Chem. Rev.*, 2023, **123**, 2112–2154.
12 A. Kamada, A. Herneke, P. Lopez-Sanchez, C. Harder, E. Ornithopoulou, Q. Wu, X. Wei, M. Schwartzkopf, P. Müller-Buschbaum, S. V. Roth, M. S. Hedenqvist, M. Langton and C. Lendel, *Nanoscale*, 2022, **14**, 2502–2510.
13 X. Ye, K. Junel, M. Gällstedt, M. Langton, X. Wei, C. Lendel and M. S. Hedenqvist, *ACS Sustain. Chem. Eng.*, 2018, **6**, 5462–5469.
14 X. Ye, A. Capezza, V. Gowda, R. T. Olsson, C. Lendel and M. S. Hedenqvist, *Adv. Sustainable Syst.*, 2021, 2100063.
15 S. G. Bolder, A. J. Vasbinder, L. M. C. Sagis and E. van der Linden, *Int. Dairy J.*, 2007, **17**, 846–853.
16 X. Ye, M. S. Hedenqvist, M. Langton and C. Lendel, *RSC Adv.*, 2018, **13**, 6915–6924.
17 M. Langton and A. M. Hermansson, *Food Hydrocolloids*, 1992, **5**, 523–539.
18 S. M. Loveday, S. G. Anema and H. Singh, *Int. Dairy J.*, 2017, **67**, 35–45.
19 A. Kamada, N. Mittal, L. D. Söderberg, T. Ingverud, W. Ohm, S. V. Roth, F. Lundell and C. Lendel, *Proc. Natl. Acad. Sci. U. S. A.*, 2017, **114**, 1232–1237.
20 A. Marchlewicz, U. Guzik and D. Wojcieszyńska, *Water, Air, Soil Pollut.*, 2015, **226**, 355.
21 J. Jan-Roblero and J. A. Cruz-Maya, *Molecules*, 2023, **28**, 2097.
22 C. Trombini, J. Blasco and M. Hampel, in *Non-Steroidal Anti-inflammatory Drugs in Water*, ed. O. Hutzinger, Springer Nature, Switzerland, 2020, vol. 96, ch. 548, pp. 161–189.
23 B. Gross, J. Montgomery-Brown, A. Naumann and M. Reinhard, *Environ. Toxicol. Chem.*, 2009, **23**, 2074–2083.
24 C. Tixier, H. P. Singer, S. Oellers and S. R. Müller, *Environ. Sci. Technol.*, 2003, **37**, 1061–1068.
25 H. J. De Lange, W. Noordoven, A. J. Murk, M. Lürling and E. T. H. M. Peeters, *Aquat. Toxicol.*, 2006, **78**, 209–216.
26 F. T. Mathias, D. H. Fockink, G. R. Disner, V. Prodocimo, J. L. C. Ribas, L. P. Ramos, M. M. Cestari and H. C. Silva de Assis, *Environ. Toxicol. Pharmacol.*, 2018, **59**, 105–113.
27 R. Sanches Pires, A. J. Capezza, M. Johansson, M. Langton and C. Lendel, Submitted, 2024.
28 M. R. Krebs, G. L. Devlin and A. M. Donald, *Biophys. J.*, 2009, **96**, 5013–5019.
29 B. Alander, A. J. Capezza, Q. Wu, E. Johansson, R. T. Olsson and M. S. Hedenqvist, *Ind. Crop. Prod.*, 2018, **119**, 41–48.

30 F. Chen, M. Gällstedt, R. T. Olsson, U. W. Gedde and M. S. Hedenqvist, *RSC Adv.*, 2015, **5**, 94191–94200.
31 B. K. Birdsong, Q. Wu, M. S. Hedenqvist, A. J. Capezza, R. L. Andersson, A. J. Svagan, O. Das, R. A. Mensah and R. T. Olsson, *Mater. Adv.*, 2024, **5**, 5041–5051.
32 H. D. Bale and P. W. Schmidt, *Phys. Rev. Lett.*, 1984, **53**, 596–599.
33 A. K. Schütz, A. Soragni, S. Hornemann, A. Aguzzi, M. Ernst, A. Böckmann and B. H. Meier, *Angew. Chem., Int. Ed.*, 2011, **50**, 5956–5960.
34 M. A. Bettelli, Q. Hu, A. J. Capezza, E. Johansson, R. T. Olsson and M. S. Hedenqvist, *Commun. Chem.*, 2024, **7**, 75.